Computational and Structural Biotechnology Journal 21 (2023) 2801–2808

Contents lists available at ScienceDirect

Computational and Structural Biotechnology Journal

journal homepage: www.elsevier.com/locate/csbj

Research article

TRIM56 coiled-coil domain structure provides insights into its E3 ligase functions

Xiaohua Lou [a], Binbin Ma [a], Yuan Zhuang [a], Xiang Xiao [a], Laurie J. Minze [a], Junji Xing [a,b], Zhiqiang Zhang [a,c], Xian C. Li [a,c,*]

[a] Immunobiology and Transplant Science Center and Department of Surgery, Houston Methodist Research Institute, Houston, TX, USA
[b] Department of Cardiovascular Sciences, Houston Methodist Research Institute, Houston, TX, USA
[c] Department of Surgery, Weill Cornell Medical College of Cornell University, New York, USA

ARTICLE INFO

Article history:
Received 11 February 2023
Received in revised form 14 April 2023
Accepted 20 April 2023
Available online 23 April 2023

Keywords:
Coiled-coil domain
Crystal structure
Tetramerization
TRIM56
E3 Ubiquitin ligase
Hydrophobic interactions

ABSTRACT

Protein ubiquitination is a post-translation modification mediated by E3 ubiquitin ligases. The RING domain E3 ligases are the largest family of E3 ubiquitin ligases, they act as a scaffold, bringing the E2-ubiquitin complex and its substrate together to facilitate direct ubiquitin transfer. However, the quaternary structures of RING E3 ligases that perform ubiquitin transfer remain poorly understood. In this study, we solved the crystal structure of TRIM56, a member of the RING E3 ligase. The structure of the coiled-coil domain indicated that the two anti-parallel dimers bound together to form a tetramer at a small crossing angle. This tetramer structure allows two RING domains to exist on each side to form an active homodimer in supporting ubiquitin transfer from E2 to its nearby substrate recruited by the C-terminal domains on the same side. These findings suggest that the coiled-coil domain-mediated tetramer is a feasible scaffold for facilitating the recruitment and transfer of ubiquitin to accomplish E3 ligase activity.

1. Introduction

Protein ubiquitination is a post-translational modification process involved in diverse conditions, in which the ubiquitin group is covalently attached to substrates through an enzymatic cascade involving E1 ubiquitin-activating enzyme, E2 ubiquitin-conjugating enzyme, and E3 ubiquitin ligases [1,2]. E3 ligases mediate the transfer of ubiquitin from an E2 ubiquitin-conjugating enzyme to its target protein substrates. Through ligation interactions, various ubiquitin linkages have been found, including mono-ubiquitination and polyubiquitination. Usually, proteins with mono-ubiquitination are involved in cellular signaling, endocytosis and DNA regulation; target proteins with Lys48-linked polyubiquitination are degraded through the proteasome pathway, whereas those with Lys63-linked ubiquitination serve as nonproteolytic cell signaling [3,4]. Based on the differences in characteristic domains and transfer mechanisms, E3 ligases can be divided into three types: homologous to E6AP carboxyl terminus (HECT) domain-containing E3 ligases (29 members in humans), RING-in-between-RING (RBR) family E3 ligases (13 members in humans), and the really interesting new gene (RING) E3 ligases (over 600 members in humans) [5–7].

The largest subfamily of RING E3 ligases is the tripartite motif protein (TRIM) family, with over 80 known protein genes in humans [8], which usually comprise a characteristic N-terminal tripartite domain motif (RBCC motif), a RING domain, one or two B-box domains, and a coiled-coil domain (CC domain). The C-terminal domains of these proteins are diverse and determine protein substrate specificity. Functional studies have indicated that TRIM family proteins play crucial roles in cellular processes, including signal transduction, innate immunity, adaptive immunity, DNA repair, differentiation, proliferation, development, apoptosis, protein quality control, autophagy, and carcinogenesis [8–12]. To exert their ubiquitin E3 ligase activity, TRIM proteins as a scaffold need to assemble a feasible quaternary structure, where RING may form a dimer and the recruited E2-Ub by the RING dimer should be in close proximity to the substrate, to accomplish the recruitment of the E2-Ub complex and direct transfer of Ub from E2-Ub to the substrate [13–18].

TRIM56, a member of the TRIM family, plays an important role in various cellular processes through its E3 ligase activity. TRIM56 may exert antiviral activity through various mechanisms. STING and cGAS

* Corresponding author at: Immunobiology and Transplant Science Center and Department of Surgery, Houston Methodist Research Institute, Houston, TX, USA.
E-mail address: xcli@houstonmethodist.org (X.C. Li).

https://doi.org/10.1016/j.csbj.2023.04.022

are key proteins in the innate immune response to viral and bacterial infections, they sense the presence of foreign DNA and trigger production of inflammatory cytokines that help fight off infections. TRIM56 interacts with STING through its C-terminal regions and promotes K63 polyubiquitination of STING, which induces STING dimerization, activates interaction with TBK1, and induces the production of IFN-β during dsDNA virus infection [19]. TRIM56 is essential for the cGAS-mediated anti-DNA virus response through direct interaction with cGAS and monoubiquitinating cGAS at K335, which enhances cGAS dimerization, DNA-binding activity, and cGAMP production [20]. Furthermore, TRIM56 restricts the infection of bovine viral diarrhea virus (BVDV), dengue virus serotype 2 (DENV2), yellow fever virus (YFV), and porcine epidemic diarrhea virus (PEDV), depending on E3 ligase activity and integrity of the C-terminal portion [21,22]. TRIM56 may also regulate tumor development through different pathways. TRIM56 may inhibit the development of ovarian cancer through Lys48-linked ubiquitination to promote the degradation of vimentin [23]. Additionally, TRIM56 may promote the proliferation of breast cancer cells through Lys63-linked ubiquitination to positively regulate the stability of the estrogen receptor α protein [24].

In contrast to extensive functional studies, structural information on TRIM56 protein is limited. The only structural study available pertains to its interaction with the bacterial effector protein, SopA. The complex structure of the SopA β-helix with TRIM56 RING domain indicates that SopA protein may hinder the interaction between the RING domain and E2 [25]. Therefore, it is unknown how the single-RING-finger TRIM56 protein structurally assembles to exert its E3 ligase activity.

In this study, we solved the crystal structure of the TRIM56 coiled-coil domain, which reveals a tetramer assembly through two dimers interacting with each other at small crossing angles. This conformation confers two N-terminal domains and two C-terminal portions at each site, which meet the two prerequisites of TRIM E3 ligase activity, including RING dimerization and the close proximity between E2-ubiqutin and its substrate. Therefore, the tetramer of the coiled-coil domain provides a structural basis for TRIM56 to facilitate the formation of its E3 ligase complex.

2. Materials and methods

2.1. Cloning, expression, and purification of the TRIM56 proteins

The DNA sequences, encoding the mouse TRIM56 (Uniprot code: Q80VI1) protein fragment 215–303 for the coiled-coil domain and 2–88 for the RING domain, were amplified by PCR. The amplified DNA fragments were cloned into a pET28-based vector, which contains a tandem tag of six consecutive histidine residues (His6) followed by a maltose-binding protein (MBP) and an HRV-3 C protease cleavage site between the tandem tag and the target protein. The constructs expressing target proteins were transformed into the BL21(DE3) strain. A single colony from an LB-agar plate containing 50 μg/mL kanamycin was inoculated into LB medium supplemented with 50 μg/mL kanamycin and then grown at 37 °C until OD_{600} reached to 0.4. The protein was then induced with 0.5 mM isopropyl-β-D-1-thiogalactopyranoside (IPTG) overnight at 18 °C. Overnight cultured cells were collected by centrifugation and washed twice with PBS. The washed cell pellets were resuspended in 500 mM NaCl, 20 mM imidazole, and 20 mM Tris pH 8.0 and lysed by sonication on ice. The insoluble portion of the cell lysate was removed by ultracentrifugation (66,200 g, 15 min) and the supernatant was loaded onto a Histrap HP column (GE Healthcare). The column was washed and eluted according to the manufacturer's instructions. The elate from the Histrap HP column was loaded onto a MBPtrap column (GE Healthcare). The column was then processed according to the manufacturer's instructions. The elate from the MBPtrap column was digested overnight with HRV-3 C protease in a 4 °C cold room. After SDS-PAGE confirmed that cleavage was complete, the cleaved His6-MBP tags were removed by passing the digested sample over a Histrap HP column. The pass-through solution containing the target protein was loaded onto a Superdex 200 column (GE Healthcare) for the final purification.

2.2. Crystallization, data collection and structure determination

The purified protein in 20 mM Tris pH8.0, 50 mM NaCl was used for crystallization. Crystallization conditions were screened by hanging-drop vapor diffusion method by mixing 0.2 μL of protein solution (6 mg/mL) with 0.2 μL of reservoir solution. Crystals grown in 10 % Glycerol, 0.1 M HEPES pH 7.5, 5 % PEG3000, and 30 % PEG400 were frozen in liquid nitrogen directly for data collection. Diffraction data were collected on the beamline 24-ID-E at the Advanced Photon Source (Chicago, IL, USA). A diffraction dataset from a single crystal was processed using Imosflm and AIMLESS software programs in the CCP4 suite [26,27]. The structure was determined using PHASER [28] in the PHENIX software package with a TRIM75 coiled-coil dimer [29] as a search model. The molecular replacement solution was further rebuilt using the PHENIX.Autobuild [30]. The rebuilt model was then refined using REFMAC5 [31] and the structure was monitored and corrected using Coot software [32] during refinement. All structural figures were prepared using PyMol software (Schrödinger, LLC). The data collection and refinement statistics are presented in Table 1.

2.3. AlphaFold2 analysis

DeepMind's open-source code AlphaFold2 was downloaded and installed as described in Github (https://github.com/deepmind/alphafold) under Linux (Ubuntu 22.04, 128 GB RAM, Nvidia RTX 3050 GPU with 8 GB RAM) [33,34]. The template parameter (–max_template_date=2022–12–14) and multimer model (–model_preset=multimer) were used for the prediction. The predicted

Table 1
Data collection and refinement statistics.

Data collection	
Space group	*I41*
Cell dimensions	
a, *b*, *c* (Å)	136.68, 136.68, 65.27
Resolution (Å)	2.80 (2.95–2.80)*
R_{merge} ♯	0.058(0.733)
$R_{p\ im}$ &	0.034(0.433)
$I/\sigma I$	9.1(1.5)
CC(1/2)	0.999(0.678)
Completeness (%)	99.4(99.2)
Redundancy	3.7(3.7)
Refinement	
Resolution (Å)	44.66–2.80
No. reflections	14151
R_{work}/R_{free}(%)Ψ	21.94/26.44
No. atoms	
Protein	2456
Ligand/ion	15
Mean B value	103
R.m.s deviations	
Bond lengths (Å)	0.007
Bond angles (°)	1.967

*Values in parentheses are for outer shell.
♯$R_{merge} = \Sigma_{hkl}\Sigma_i\ |I_i\ (hkl) - < I(hkl) > |/\Sigma_{hkl}\ \Sigma_i\ I_i(hkl)$, where $I_{\ i}\ (hkl)$ is the intensity of reflection i and $< I(hkl) >$ is the average intensity of all reflections with indices hkl.
&$R_{\text{pim}} = \Sigma_{hkl}\ [1/(\text{N-1})]^{1/2}\Sigma_{\ i}\ |I_{\ i}\ (hkl) - < I(hkl) > |/\ \Sigma_{hkl}\ \Sigma_i\ I_{\ i}\ (hkl)$.
Ψ$R_{\text{work}} = \Sigma_{hkl}\ |\ |F_{\text{obs}}\ (hkl)| - |F_{calc}\ (hkl)|\ |/\Sigma_{\ hkl}\ |F_{\text{obs}}(hkl)|$; R_{free} was calculated using 5 % of data.

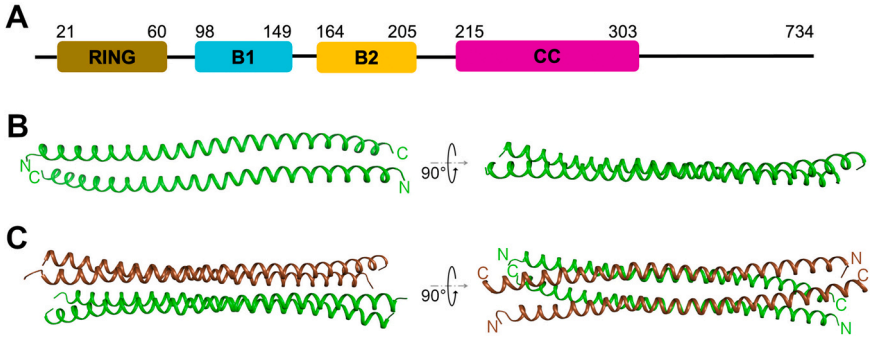

Fig. 1. Overall crystal structure of the TRIM56 coiled-coil domain. (A) Schematic representation of domain organization of TRIM56 protein. B1, B box 1; B2, B box 2; CC, the coiled-coil domain. The residue boundaries of the domains are indicated. The coiled-coil domain is colored in magenta. (B, C) Cartoon representation of (B) an antiparallel dimer and (C) a tetramer in two vertical views.

structures were evaluated based on PAE and pLDDT. Ten top-ranked structures were inspected using PyMol software.

2.4. SEC-MALS assay

The molar mass of the purified proteins in solution was measured using multi-angle light scattering coupled with size exclusion chromatography (SEC-MALS) in the Core for Biomolecular Structure and Function (CBSF) at the University of Texas MD Anderson Cancer Center, Houston, Texas. The SEC-MALS system comprised HPLC, including a differential refractive index detector and a WTC-010S5 column (Wyatt Technology Co. Ltd.), and MALS with an 18-angle static scattering detector. BSA was used as a calibration standard and phosphate-buffered saline (PBS) was used as the running buffer. Purified coiled-coil protein (40 µL) at a concentration of 6 mg/mL was loaded onto the system for molar mass analysis at room temperature. The data were processed using ASTRA software (Wyatt Technology).

2.5. Chemical cross-linking assay

The mouse TRIM56 cDNA (Uniprot code: Q80VI1) fused with an N-terminal FLAG-tag was inserted into the multiple cloning site (MCS) region under the control of the CMV promoter in the pBudCE4.1 vector (Invitrogen). The expression construct was transfected into HEK293T cells in a 100 mm cell culture dish using Lipofectamine 3000 (Invitrogen), according to the manufacturer's instructions. After two days of incubation, the cells were rinsed with PBS and lysed with RIPA buffer containing EDTA-free protease inhibitor cocktail (Roche) on ice. FLAG-tagged proteins were extracted from clear lysate using anti-FLAG magnetic agarose (Pierce). Then, the magnetic agarose was washed with washing buffer (20 mM tris pH 7.5, 500 mM NaCl, 0.5 % TWEEN 20, and EDTA-free protease inhibitor cocktail). After washing thrice, the FLAG-tagged proteins were eluted with 1 × FLAG peptide (0.2 mg/mL) in PBS supplemented with EDTA-free protease inhibitor cocktail. The FLAG peptide left in the elute was then removed using a 0.5 mL Zeba spin desalting column (Pierce). The purification was performed in a cold room. The purified sample was aliquoted into five tubes for the glutaraldehyde cross-linking assay. Freshly diluted 0, 10, 20, 40, and 80 mM glutaraldehyde stocks in PBS were added to the five samples at final concentrations of 0, 1, 2, 4, and 8 mM, respectively. The protein-glutaraldehyde mixtures were reacted for five minutes at 22 ℃ room temperature and then the reaction was terminated immediately by adding a saturated glycine solution [35,36]. The freshly quenched cross-linked samples were immediately resolved by SDS-PAGE on 4–15 % Mini-PROTEAN TGX Precast Protein Gels (Bio-Rad) under reducing conditions, and FLAG-tagged TRIM56 proteins were visualized by western blotting with an anti-FLAG antibody (Sigma, Cat#F1804).

2.6. DNA mutagenesis

Mutants of full-length TRIM56, and TRIM56 coiled-coil domain were produced using site-directed mutagenesis. The constructs were confirmed by DNA sequencing.

2.7. In vitro ubiquitination assay

The expression plasmid of Flag-tagged wild-type or mutant full-length TRIM56 (2500 ng) was transfected into 1 × 10^6 HEK293T cells seeded on a well of 6-well plate. After two days, the full-length proteins were isolated using anti-Flag magnetic beads (Pierce) and then mixed with the reaction mixture containing 300 mM Ube1 from the Ubiquitin Thioester/Conjugation Initiation kit (K-995, BostonBiochem), 3uM E2 (UbcH5a, UbcH5b, or UbcH7) from UbcH Enzyme set (K-980, BostonBiochem), 50uM Ub, and 2.5 mM ATP in the reaction buffer (50 mM NaCl, 5 mM $MgCl_2$, 0.5 mM DTT, and 50 mM Tris pH7.6). The reaction was stopped after 1.5 h of incubation at 37 ℃ by the addition of SDS-PAGE sample loading buffer. The samples were resolved by SDS-PAGE and analyzed by western blotting.

3. Results

3.1. Overall crystal structure of TRIM56 coiled-coil domain

TRIM56 is a member of the TRIM subfamily that contains the RING domain, B box 1, B box 2, coiled-coil domain, and a C-terminal region. The mouse TRIM56 coiled-coil domain ranging from amino acids 215–303 was crystallized (Fig. 1A). The structure was solved at 2.80 Å, with four molecules in the asymmetric unit. The statistics for collection and refinement are presented in Table 1. Packing analysis indicated that the four molecules in the asymmetric unit form two antiparallel dimers (Fig. 1B); then, the two antiparallel dimers bind together with a small crossing angle to form a proximately antiparallel tetramer (Fig. 1C).

3.2. Detailed interactions involved in tetramerization of the TRIM56 coiled-coil domain

First, the dimerization interface between the two antiparallel chains was analyzed. The results showed that ample hydrophobic residues, including L230, L241, L244, A248, V251, V255, I262 L263, L266, L267, V273, L274, L277, L280, V281, and I295, exist on the dimerization interface, and they form five discontinuous hydrophobic regions by interacting with those from the partner chain (Fig. 2A). In

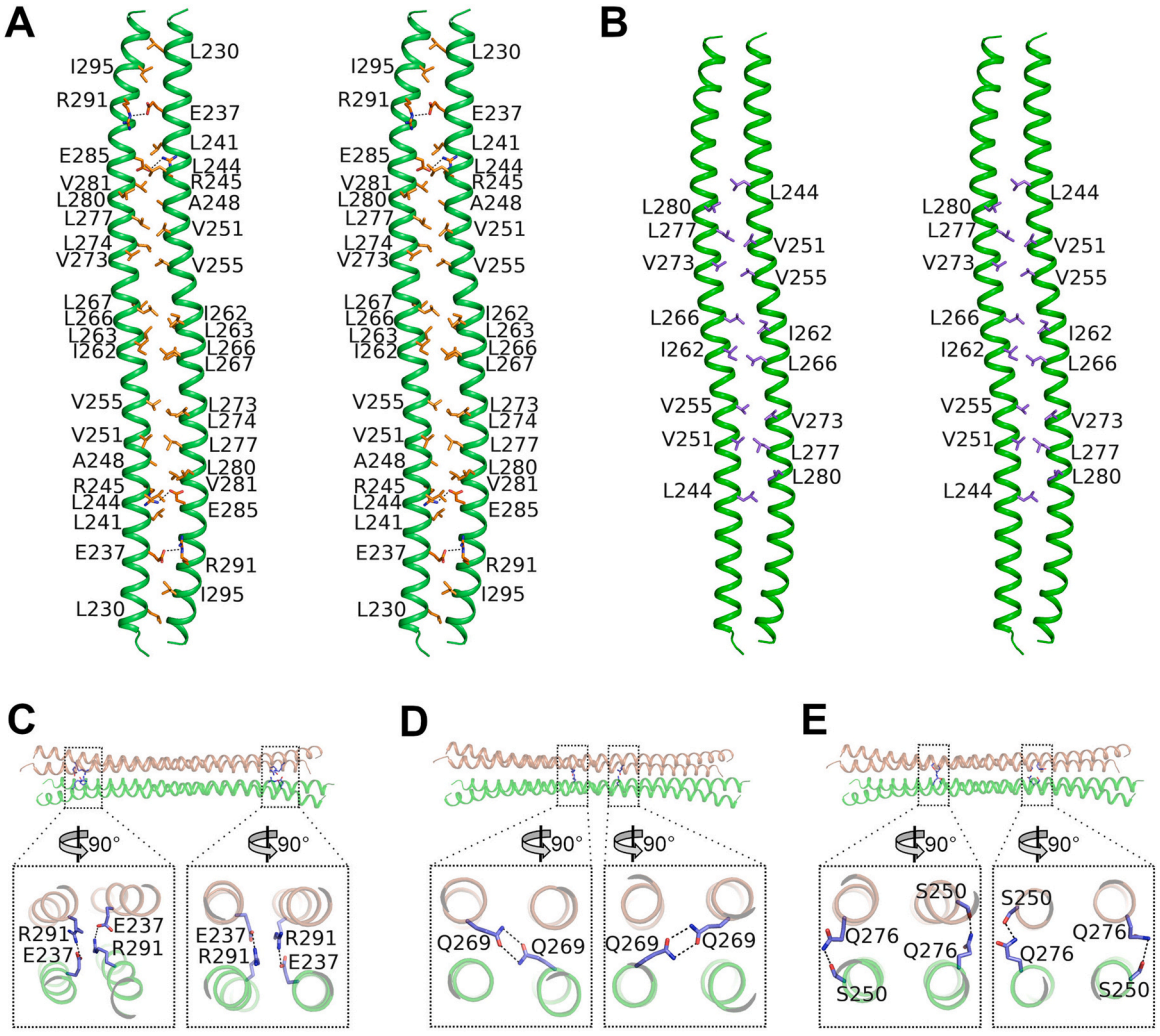

Fig. 2. Detailed interactions involved in the tetramer formation. (A) Stereo view of the interactions involved in the dimerization of two antiparallel helices. The two helices are shown as a ribbon diagram. The side chains of the residues on the dimerization interface are presented as sticks. Salt bridges are indicated by dashed lines. (B) Stereo view of hydrophobic residues located in the tetramerization interface. The side chains of the hydrophobic residues are shown in purple sticks. (C) Salt bridges between E237 and R291 link the two dimers among a tetramer. The two dimers are shown in brown and green, respectively. The positions of the salt bridges were indicated by two rectangles in the tetramer and the detailed interactions were shown in enlarged sections. (D) Hydrogen bonds formed between two Q269 link the two dimers. (E) Hydrogen bonds between S250 and Q276 link the two dimers.

addition to the dominant hydrophobic interactions, four interchain salt bridges, two formed between E285 and R245 and the other two between R291 and E237, continually strengthened the dimerization (Fig. 2A).

Next, the dimer surface that takes part in binding with another dimer to form a tetramer was analyzed. On this surface, hydrophobic residues including L244, V251, V255, I262, L266, V273, L277, and L280 in the central region from one dimer may interact with those from another dimer (Fig. 2B). The buried surface area and energy of solvation that contributed to the binding of the two dimers were analyzed using the EMBL-EBI PISA service [37]. The results indicated that the coiled-coil domain may form a stable tetramer in solution, where the buried surface area of the tetramerization interface is 5350 Å^2, the solvation free energy gain upon formation of the whole tetramer is −96.6 kcal/mol, and the solvation free energy gain upon tetramerization through two dimers is −27.9 kcal/mol (Table 2). In addition to the hydrophobic interactions located in the central region, salt bridges and hydrogen bonds are also found in the tetramerization interface. R291 and E237 form four interchain salt bridges (Fig. 2C). The side chains of Q269 may form interchain hydrogen bonds (Fig. 2D), and the side chains of S250 and Q276 may form four outer interchain hydrogen bonds between the two dimers (Fig. 2E). These salt bridges and hydrogen bonds continually strengthen tetramerization, which is dominated by hydrophobic interactions. All residues, except S250 and L280, involved in the formation of the coiled-coil tetramer, are highly conserved among different species (Fig. S1).

Table 2
Assembly Analysis by *PISA*.

Composition (Chains)	Surface area (Å^2)	Buried surface area(Å^2)	ΔG^{int*} (kcal/mol)	$\Delta G^{diss\sharp}$ (Kcal/mol)
ABCD	17880	11670	-96.6	24.1
AB	11600	3220	-34.8	27.2
CD	11630	3110	-32.9	23.0
AD	12470	2270	-11.1	4.8
BC	12640	2180	-11.6	3.3

*ΔG^{int} indicates the solvation free energy gain upon formation of the assembly.
#ΔG^{diss} indicates the free energy of assembly dissociation.

3.3. Comparison with AlphaFold2 predicting tetramer structure

The tetramer structure of the TRIM56 coiled-coil domain was predicted using the AlphaFold2-multimer. In the predicted structure,

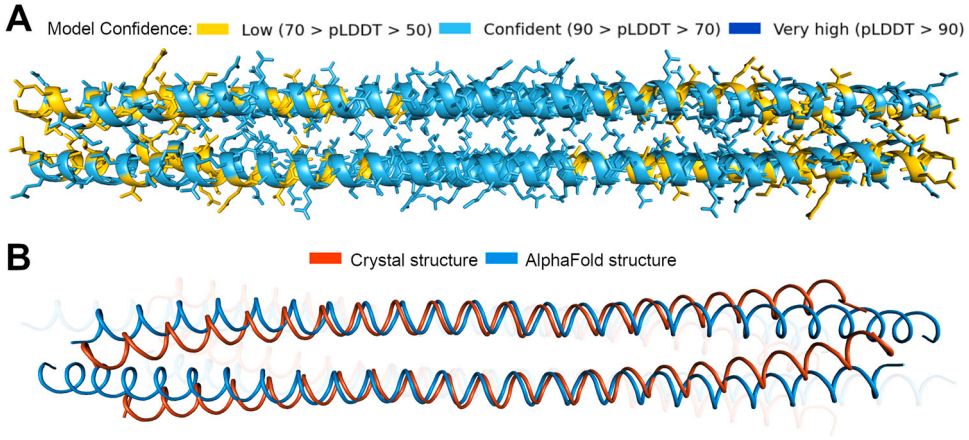

Fig. 3. Comparison between the crystal structure and AlphaFold2 predicted model. (A) AlphaFold2 predicted coiled-coil tetramer model. (B) Superposition of the crystal structure and the AlphaFold2 predicted model. The central portions from A249 to A279 were superposed between the two tetramers. The back dimers of the two tetramers were made transparent for clarity.

the central part of the tetramer was confident and the two distal structures were less confident (Fig. 3A). The predicted structure was then compared to the structure obtained from our crystallographic analysis in the present study. After superposing the central portions from A249 to A279 of the two tetramers (Fig. 3B), we observed that the central portions between the two structures fit well (RMSD:1.327), while the two distal portions showed clear differences. This result indicates that the central portion of the tetramer, which is dominated by hydrophobic interactions, may be predicted by AlphaFold2.

3.4. Tetrameric assembly in solution

SEC-MALS was used to confirm the oligomeric state of the coiled-coil domain in solution. The results showed that the purified protein of the coiled-coil domain was ~40 kDa in PBS, consistent with the theoretical molecular weight of a tetramer (40.07 kDa) (Fig. 4A). This finding suggests that the tetramer is the basic oligomeric state of this domain. Next, we mutated the residues involved in tetramerization (Fig. 2B-E), SEC-MALS analysis indicated that the mutant (L244A, V251A, V255A, I262A, L266A, Q269A, V273A, Q276A, L277A,

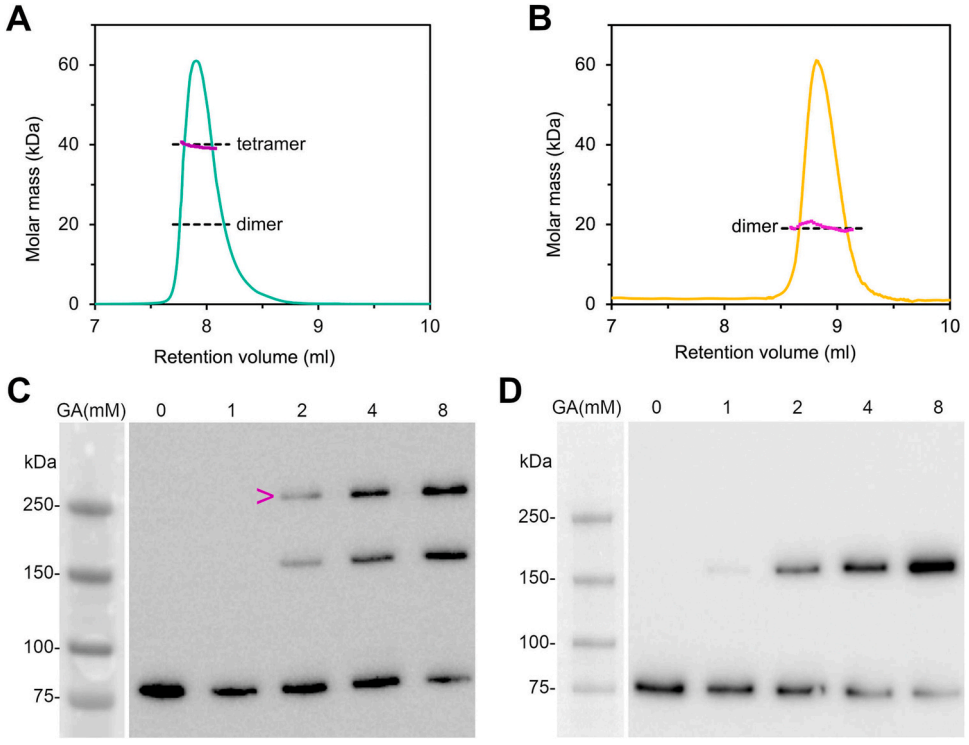

Fig. 4. Assembly analysis of TRIM56 in solution. (A) SEC-MALS measurement of the purified TRIM56 coiled-coil domain protein. The measured molar mass of the elution peak is indicated in magenta. The dimer (20.04 kDa) and tetramer (40.07 kDa) masses calculated from the protein sequence are indicated with black dashed lines. (B) SEC-MALS measurement of the mutated coiled-coil protein. The mutant protein contains eleven alanine substitutions in the coiled-coil region that disrupt its ability to tetramerize. (C) Cross-linking analysis of full-length protein expressed in HEK293T cells. Protein markers are shown at the left lane. The concentrations of glutaraldehyde (GA) are indicated at the top of the panel. The theoretical monomer and tetramer masses are 80.71 kDa and 322.84 kDa, respectively. The predicted tetramer band is indicated by a magenta arrow. (D) Cross-linking analysis of full-length protein with eleven mutations in the coiled-coil region expressed in HEK293T cells. The theoretical monomer mass of the mutant is 80.22 kDa.

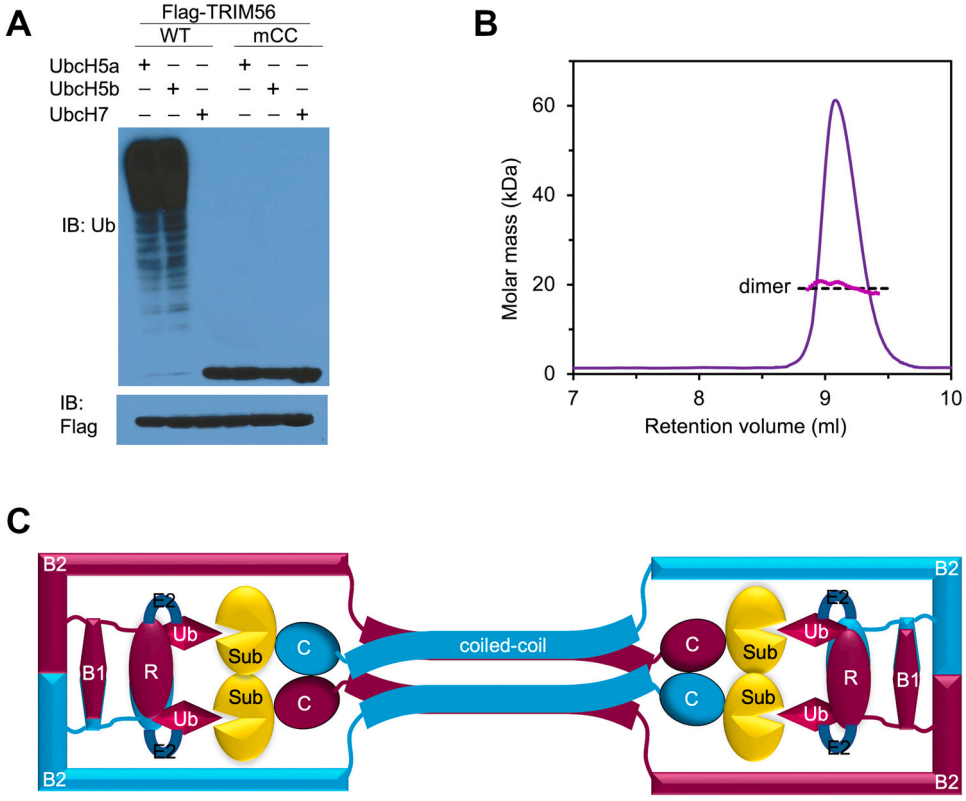

Fig. 5. Coiled-coil tetramer scaffold facilitates the complex formation of TRIM56 E3 ligase activity. (A) Ubiquitin E3 ligase activity analysis of two TRIM56 proteins. The wild-type full-length TRIM56 protein is labeled as WT, while the full-length TRIM56 protein with a mutation of the eleven residues in the coiled-coil region is labeled as mCC. (B) SEC-MALS analysis of the purified TRIM56 RING domain. This RING protein ranges from N2 to A88, which includes N- and C-terminal helices. The measured molar mass of the elution peak is indicated in magenta. The dimer (19.18 kDa) mass calculated from the protein sequence is indicated with black dashed lines. (C) Model of a tetrameric E3 ligase complex mediated by the coiled-coil domain. The quaternary conformation may promote the formation of homodimers of RING (R), B box 1 (B1), B box 2 (B2), and C-terminal domain (C) on the same side. The E2-Ub complex recruited by the RING dimer may be in close proximity to the substrate (Sub) recruited by the C-terminal domain, facilitating the direct transfer of Ub from the E2-Ub complex to the substrate.

L280A, R291A) only formed a dimer in solution (Fig. 4B). These results indicate that those residues indeed play a critical role in the tetramerization process.

3.5. Tetrameric assembly of full-length TRIM56 protein

To investigate the oligomeric state of full-length TRIM56 protein, a cross-linking method was used to detect oligomers of full-length proteins expressed in HEK293T cells. The protein extracted from the lysate of FLAG-tagged TRIM56-expressing HEK293T cells was cross-linked with different concentrations of glutaraldehyde. Western blot analysis of the cross-linked samples showed that a tetramer band was present for the wild-type protein in the extracted sample (Fig. 4C). However, no tetramer band was detected for full-length protein with the mutation of the eleven tetramerization-associated residues in coiled-coil region (Fig. 4D). These results suggest that the coiled-coil domain plays a critical role in promoting tetramer formation of the full-length TRIM56 protein.

3.6. Proposed model of TRIM56 ubiquitin E3 ligase activity

We investigated the E3 ligase activities of both the wild-type and mutant full-length TRIM56 proteins. Our results showed that the wild-type protein could activate ubiquitination of ubiquitin in the presence of UbcH5a or UbcH5b, but not UbcH7 (Fig. 5A). However, no ubiquitination product was detected for the mutant protein (Fig. 5A). This finding suggested that tetramerization is necessary for TIRM56 to perform its E3 ligase activity. Additionally, SEC-MALS measurement suggested that the RING domain could form a dimer in solution (Fig. 5B).

Based on the structural and other auxiliary analysis of the TRIM56 protein, once two antiparallel coiled-coil dimers bind together to form a tetramer shown in the TRIM56 structure, two close C-terminal ends and two close N-terminal ends exist at each side of the tetramer (Fig. 1C). Therefore, there are two RING domains, two B box 1 and two B box 2, on the same side of the full-length protein, which may facilitate the formation of a RING dimer, B box 1 dimer, and B box 2 dimer in space (Fig. 5C). Similarly, two C-terminal domains exist on each side of the tetramer, which may facilitate the recruitment of substrate dimers and then present them to the closed RING-E2-Ub complex to accomplish the direct transfer of Ub from the E2-Ub complex to the substrate (Fig. 5C).

4. Discussion

4.1. Hydrophobic interactions are a common feature of coiled-coil domain dimerization

In this TRIM56 structure, hydrophobic interactions dominated the dimerization of two chains of an antiparallel dimer (Fig. 2A). Similar hydrophobic interactions also exist in other reported TRIM coiled-coiled dimeric structures, such as TRIM5 [38,39], TRIM20 [40], TRIM25 [41,42], TRIM28 [43–45], and TRIM69 [46]. Therefore, hydrophobic interactions are a common feature of TRIM proteins, which bind two chains together to form an antiparallel dimer.

4.2. Coiled-coil domain may mediate tetramerization with different interaction patterns

We previously reported that the TRIM75 coiled-coil domain forms a tetramer through two disulfide bonds and other interactions [29]. In this TRIM56 structure, besides some salt bridges and hydrogen bonds, hydrophobic interactions mainly contribute to tetramerization. Sequence alignment suggested that hydrophobic residues exist extensively on the hydrophobic face in various TRIM members [29]. Therefore, hydrophobic interactions that dominate tetramerization of the coiled-coil domain could exist in other TRIM members. Although both structures form tetramers, their structures exhibit clear differences owing to their different interaction patterns. Therefore, this is another interaction pattern for the tetramerization of the coiled-coil domain.

4.3. The coiled-coil domain tetramerization facilitates the formation of stable complex through synergized interactions

Among the tetrameric model derived from the coiled-coil domain, besides the binding affinity generated from the coiled-coil domain, the binding affinity generated from RING dimer, B box 1 dimer and B box 2 dimer at each side may also synergistically stabilize the tetramer. Here, our SEC-MALS experiment indicated that the RING domain containing N- and C-terminal helices formed a dimer in solution (Fig. 5B). Furthermore, dimerization of analogous RING domains or B boxes has also been reported in other TRIM members [16,47–51]. This synergistic cooperation may help explain why fragments containing the B box and coiled-coil domain promote homomultimerization of TRIM63 and TRIM27 [47,52]. Furthermore, tetramer assemblies in solution have been identified in various multidomain TRIM proteins [15,16,43]. Therefore, the proposed tetramer model may explain the formation of the TRIM56 E3 ligase complex through synergistic cooperation among the domains. However, further studies are required to verify and improve the proposed tetramer model based on full-length proteins and/or their complexes.

In summary, this study revealed that the coiled-coil domain of TRIM56 forms a tetramer via a unique interaction pattern. This tetramer structure allows full-length TRIM56 to form a stable tetramer and facilitates the formation of the TRIM E3 ligase complex and the direct transfer of Ub from the Ub-E2 complex to protein substrates. Overall, this study provides structural insights into the mechanism underlying TRIM56 E3 ligase activity. Therefore, further functional studies may allow the development of therapeutic strategies targeting TRIM56 for therapeutic purposes.

Accession numbers

The atomic coordinates and structure factors were deposited in the Protein Data Bank (www.wwpdb.org) with access code 8FXF.

CRediT authorship contribution statement

Xiaohua Lou: Conceptualization, Investigation, Software, Data curation, supervision, visualization, writing – original draft, writing – review, and editing. **Binbin Ma:** Investigation, Data curation, and visualization. **Yuan Zhuang:** Investigation, Visualization. **Xiang Xiao**, Investigation. **Laurie J. Minze**. Investigation. **Junji Xing**: Investigation, visualization. **Zhiqiang Zhang**: Conceptualization, Supervision, Writing – review and editing, and funding acquisition. **Xian C. Li**: Conceptualization, Project administration, writing – review and editing, Supervision, Funding acquisition.

Declaration of Competing Interest

None.

Acknowledgments

We thank Paul Leonard and Troy Johnson in Biomolecular Structure and Function Core at the MD Anderson Cancer Center for their help with SEC-MALS analysis. In this study, the 24-ID-E beam line (GM124165) and an Eiger detector (OD021527) were used at the APS (DE-AC02–06CH11357). This project was supported in part by the American Heart Association Career Development Award, USA (20CDA35260116 to Junji Xing), the National Institutes of Health (NIH) grants, USA (R01 AI080779 to Xian C. Li and R01 AI155488 to Zhiqiang Zhang).

Appendix A. Supporting information

Supplementary data associated with this article can be found in the online version at doi:10.1016/j.csbj.2023.04.022.

References

[1] Swatek KN, Komander D. Ubiquitin modifications. Cell Res 2016;26:399–422. https://doi.org/10.1038/cr.2016.39
[2] Hershko A, Ciechanover A. The ubiquitin system. Annu Rev Biochem 1998;67:425–79. https://doi.org/10.1146/annurev.biochem.67.1.425
[3] Miranda M, Sorkin A. Regulation of receptors and transporters by ubiquitination: new insights into surprisingly similar mechanisms. Mol Inter 2007;7:157–67. https://doi.org/10.1124/mi.7.3.7
[4] Kravtsova-Ivantsiv Y, Ciechanover A. Non-canonical ubiquitin-based signals for proteasomal degradation. J Cell Sci 2012;125:539–48. https://doi.org/10.1242/jcs.093567
[5] Smit JJ, Sixma TK. RBR E3-ligases at work. EMBO Rep 2014;15:142–54. https://doi.org/10.1002/embr.201338166
[6] Deshaies RJ, Joazeiro CAP. RING domain E3 ubiquitin ligases. Annu Rev Biochem 2009;78:399–434. https://doi.org/10.1146/annurev.biochem.78.101807.093809
[7] Rotin D, Kumar S. Physiological functions of the HECT family of ubiquitin ligases. Nat Rev Mol Cell Biol 2009;10:398–409. https://doi.org/10.1038/nrm2690
[8] van Gent M, Sparrer KMJ, Gack MU. TRIM Proteins and their roles in antiviral host defenses. Annu Rev Virol 2018;5:385–405. https://doi.org/10.1146/annurev-virology-092917-043323
[9] Ozato K, Shin D-M, Chang T-H, Morse HC. TRIM family proteins and their emerging roles in innate immunity. Nat Rev Immunol 2008;8:849–60. https://doi.org/10.1038/nri2413
[10] Hatakeyama S. TRIM Family proteins: roles in autophagy, immunity, and carcinogenesis. Trends Biochem Sci 2017;42:297–311. https://doi.org/10.1016/j.tibs.2017.01.002
[11] Zhang L, Afolabi LO, Wan X, Li Y, Chen L. Emerging roles of tripartite motif-containing family proteins (TRIMs) in eliminating misfolded proteins. Front Cell Dev Biol 2020:8.
[12] Yang W, Gu Z, Zhang H, Hu H. To TRIM the immunity: from innate to adaptive immunity. Front Immunol 2020:11.
[13] Fiorentini F, Esposito D, Rittinger K. Does it take two to tango? RING domain self-association and activity in TRIM E3 ubiquitin ligases. Biochem Soc Trans 2020;48:2615–24. https://doi.org/10.1042/BST20200383
[14] Kiss L, Zeng J, Dickson CF, Mallery DL, Yang J-C, McLaughlin SH, et al. A tri-ionic anchor mechanism drives Ube2N-specific recruitment and K63-chain ubiquitination in TRIM ligases. Nat Commun 2019;10:4502. https://doi.org/10.1038/s41467-019-12388-y
[15] Sanchez JG, Chiang JJ, Sparrer KMJ, Alam SL, Chi M, Roganowicz MD, et al. Mechanism of TRIM25 catalytic activation in the antiviral RIG-I pathway. Cell Rep 2016;16:1315–25. https://doi.org/10.1016/j.celrep.2016.06.070
[16] Koliopoulos MG, Esposito D, Christodoulou E, Taylor IA, Rittinger K. Functional role of TRIM E3 ligase oligomerization and regulation of catalytic activity. EMBO J 2016;35:1204–18. https://doi.org/10.15252/embj.201593741
[17] Metzger MB, Pruneda JN, Klevit RE, Weissman AM. RING-type E3 ligases: master manipulators of E2 ubiquitin-conjugating enzymes and ubiquitination. Biochim Biophys Acta 2014;1843:47–60. https://doi.org/10.1016/j.bbamcr.2013.05.026
[18] Morreale FE, Walden H. Types of Ubiquitin Ligases. 248-248.e1 Cell 2016;165. https://doi.org/10.1016/j.cell.2016.03.003
[19] Tsuchida T, Zou J, Saitoh T, Kumar H, Abe T, Matsuura Y, et al. The ubiquitin ligase TRIM56 regulates innate immune responses to intracellular double-stranded DNA. Immunity 2010;33:765–76. https://doi.org/10.1016/j.immuni.2010.10.013
[20] Seo GJ, Kim C, Shin W-J, Sklan EH, Eoh H, Jung JU. TRIM56-mediated monoubiquitination of cGAS for cytosolic DNA sensing. Nat Commun 2018;9:613. https://doi.org/10.1038/s41467-018-02936-3

[21] Wang J, Liu B, Wang N, Lee Y-M, Liu C, Li K. TRIM56 is a virus- and interferon-inducible E3 ubiquitin ligase that restricts pestivirus infection. J Virol 2011;85:3733–45. https://doi.org/10.1128/JVI.02546-10
[22] Liu B, Li NL, Wang J, Shi P-Y, Wang T, Miller MA, et al. Overlapping and distinct molecular determinants dictating the antiviral activities of TRIM56 against flaviviruses and coronavirus. J Virol 2014;88:13821–35. https://doi.org/10.1128/JVI.02505-14
[23] Zhao L, Zhang P, Su X-J, Zhang B. The ubiquitin ligase TRIM56 inhibits ovarian cancer progression by targeting vimentin. J Cell Physiol 2018;233:2420–5. https://doi.org/10.1002/jcp.26114
[24] Xue M, Zhang K, Mu K, Xu J, Yang H, Liu Y, et al. Regulation of estrogen signaling and breast cancer proliferation by an ubiquitin ligase TRIM56. Oncogenesis 2019;8:30. https://doi.org/10.1038/s41389-019-0139-x
[25] Fiskin E, Bhogaraju S, Herhaus L, Kalayil S, Hahn M, Dikic I. Structural basis for the recognition and degradation of host TRIM proteins by Salmonella effector SopA. Nat Commun 2017;8:14004. https://doi.org/10.1038/ncomms14004
[26] Battye TGG, Kontogiannis L, Johnson O, Powell HR, Leslie AGW. iMOSFLM: a new graphical interface for diffraction-image processing with MOSFLM. Acta Crystallogr D Biol Crystallogr 2011;67:271–81. https://doi.org/10.1107/S0907444910048675
[27] Winn MD, Ballard CC, Cowtan KD, Dodson EJ, Emsley P, Evans PR, et al. Overview of the CCP4 suite and current developments. Acta Crystallogr D Biol Crystallogr 2011;67:235–42. https://doi.org/10.1107/S0907444910045749
[28] McCoy AJ, Grosse-Kunstleve RW, Adams PD, Winn MD, Storoni LC, Read RJ. Phaser crystallographic software. J Appl Crystallogr 2007;40:658–74. https://doi.org/10.1107/S0021889807021206
[29] Lou X, Ma B, Zhuang Y, Xiao X, Minze LJ, Xing J, et al. Structural studies of the coiled-coil domain of TRIM75 reveal a tetramer architecture facilitating its E3 ligase complex. Comput Struct Biotechnol J 2022;20:4921–9. https://doi.org/10.1016/j.csbj.2022.08.069
[30] Terwilliger TC, Grosse-Kunstleve RW, Afonine PV, Moriarty NW, Zwart PH, Hung LW, et al. Iterative model building, structure refinement and density modification with the PHENIX AutoBuild wizard. Acta Crystallogr D Biol Crystallogr 2008;64:61–9. https://doi.org/10.1107/S090744490705024X
[31] Murshudov GN, Skubák P, Lebedev AA, Pannu NS, Steiner RA, Nicholls RA, et al. REFMAC5 for the refinement of macromolecular crystal structures. Acta Crystallogr D Biol Crystallogr 2011;67:355–67. https://doi.org/10.1107/S0907444911001314
[32] Emsley P, Cowtan K. Coot: model-building tools for molecular graphics. Acta Crystallogr D Biol Crystallogr 2004;60:2126–32. https://doi.org/10.1107/S0907444904019158
[33] Jumper J, Evans R, Pritzel A, Green T, Figurnov M, Ronneberger O, et al. Highly accurate protein structure prediction with AlphaFold. Nature 2021;596:583–9. https://doi.org/10.1038/s41586-021-03819-2
[34] Evans R., O'Neill M., Pritzel A., Antropova N., Senior A., Green T., et al. Protein complex prediction with AlphaFold-Multimer 2021:2021.10.04.463034. ⟨https://doi.org/10.1101/2021.10.04.463034⟩.
[35] Li X, Sodroski J. The TRIM5α B-Box 2 domain promotes cooperative binding to the retroviral capsid by mediating higher-order self-association. J Virol 2008;82:11495–502. https://doi.org/10.1128/JVI.01548-08
[36] Javanbakht H, Yuan W, Yeung DF, Song B, Diaz-Griffero F, Li Y, et al. Characterization of TRIM5alpha trimerization and its contribution to human immunodeficiency virus capsid binding. Virology 2006;353:234–46. https://doi.org/10.1016/j.virol.2006.05.017
[37] Krissinel E, Henrick K. Inference of macromolecular assemblies from crystalline state. J Mol Biol 2007;372:774–97. https://doi.org/10.1016/j.jmb.2007.05.022
[38] Keown JR, Black MM, Ferron A, Yap M, Barnett MJ, Pearce FG, et al. A helical LC3-interacting region mediates the interaction between the retroviral restriction factor Trim5α and mammalian autophagy-related ATG8 proteins. J Biol Chem 2018;293:18378–86. https://doi.org/10.1074/jbc.RA118.004202
[39] Goldstone DC, Walker PA, Calder LJ, Coombs PJ, Kirkpatrick J, Ball NJ, et al. Structural studies of postentry restriction factors reveal antiparallel dimers that enable avid binding to the HIV-1 capsid lattice. Proc Natl Acad Sci USA 2014;111:9609–14. https://doi.org/10.1073/pnas.1402448111
[40] Weinert C, Morger D, Djekic A, Grütter MG, Mittl PRE. Crystal structure of TRIM20C-terminal coiled-coil/B30.2 fragment: implications for the recognition of higher order oligomers. Sci Rep 2015;5:10819. https://doi.org/10.1038/srep10819
[41] Koliopoulos MG, Lethier M, van der Veen AG, Haubrich K, Hennig J, Kowalinski E, et al. Molecular mechanism of influenza A NS1-mediated TRIM25 recognition and inhibition. Nat Commun 2018;9:1820. https://doi.org/10.1038/s41467-018-04214-8
[42] Sanchez JG, Okreglicka K, Chandrasekaran V, Welker JM, Sundquist WI, Pornillos O. The tripartite motif coiled-coil is an elongated antiparallel hairpin dimer. Proc Natl Acad Sci USA 2014;111:2494–9. https://doi.org/10.1073/pnas.1318962111
[43] Stoll GA, Oda S-I, Chong Z-S, Yu M, McLaughlin SH, Modis Y. Structure of KAP1 tripartite motif identifies molecular interfaces required for retroelement silencing. Proc Natl Acad Sci USA 2019;116:15042–51. https://doi.org/10.1073/pnas.1901318116
[44] Stoll GA, Pandiloski N, Douse CH, Modis Y. Structure and functional mapping of the KRAB-KAP1 repressor complex. EMBO J 2022;41:e111179. https://doi.org/10.15252/embj.2022111179
[45] Lim M, Newman JA, Williams HL, Masino L, Aitkenhead H, Gravard AE, et al. A ubiquitin-binding domain that binds a structural fold distinct from that of ubiquitin. Struct Lond Engl 1993 2019;27:1316–25. https://doi.org/10.1016/j.str.2019.05.003
[46] Li Y, Wu H, Wu W, Zhuo W, Liu W, Zhang Y, et al. Structural insights into the TRIM family of ubiquitin E3 ligases. Cell Res 2014;24:762–5. https://doi.org/10.1038/cr.2014.46
[47] Mrosek M, Meier S, Ucurum-Fotiadis Z, von Castelmur E, Hedbom E, Lustig A, et al. Structural analysis of B-Box 2 from MuRF1: identification of a novel self-association pattern in a RING-like fold. Biochemistry 2008;47:10722–30. https://doi.org/10.1021/bi800733z
[48] Keown JR, Yang J, Black MM, Goldstone DC. The RING domain of TRIM69 promotes higher-order assembly. Acta Crystallogr Sect Struct Biol 2020;76:954–61. https://doi.org/10.1107/S2059798320010499
[49] Huang S-Y, Naik MT, Chang C-F, Fang P-J, Wang Y-H, Shih H-M, et al. The B-box 1 dimer of human promyelocytic leukemia protein. J Biomol NMR 2014;60:275–81. https://doi.org/10.1007/s10858-014-9869-4
[50] Sun Y, Keown JR, Black MM, Raclot C, Demarais N, Trono D, et al. A Dissection of Oligomerization by the TRIM28 Tripartite Motif and the Interaction with Members of the Krab-ZFP Family. J Mol Biol 2019;431:2511–27. https://doi.org/10.1016/j.jmb.2019.05.002
[51] Dickson C, Fletcher AJ, Vaysburd M, Yang J-C, Mallery DL, Zeng J, et al. Intracellular antibody signalling is regulated by phosphorylation of the Fc receptor TRIM21. ELife 2018;7:e32660. https://doi.org/10.7554/eLife.32660
[52] Cao T, Borden KL, Freemont PS, Etkin LD. Involvement of the rfp tripartite motif in protein-protein interactions and subcellular distribution. J Cell Sci 1997;110(Pt 14):1563–71. https://doi.org/10.1242/jcs.110.14.1563